Half-of-the-Sites Binding of Reactive Intermediates and Their Analogues to 4-Oxalocrotonate Tautomerase and Induced Structural Asymmetry of the Enzyme†

Hugo F. Azurmendi,‡ Scott G. Miller,§ Christian P. Whitman,*,§ and Albert S. Mildvan*,‡

Department of Biological Chemistry, The Johns Hopkins School of Medicine, 725 North Wolfe Street, Baltimore, Maryland 21205-2185, and Division of Medicinal Chemistry, College of Pharmacy, The University of Texas, Austin, Texas 78712-1074

Received February 11, 2005; Revised Manuscript Received April 5, 2005

ABSTRACT: 4-Oxalocrotonate tautomerase (4-OT), a homohexameric enzyme, converts the unconjugated enone, 2-oxo-4-hexenedioate (**1**), to the conjugated enone, 2-oxo-3-hexenedioate (**3**), via a dienolic intermediate, 2-hydroxymuconate (**2**). Pro-1 serves as the general base, and both Arg-11 and Arg-39 function in substrate binding and catalysis in an otherwise hydrophobic active site. Although 4-OT exhibits hyperbolic kinetics and no structural asymmetry either by X-ray or by NMR, inactivation by two affinity labels showed half-site stoichiometry [Stivers, J. T., et al. (1996) *Biochemistry 35*, 803−813; Johnson, W. H., Jr., et al. (1997) *Biochemistry 36*, 15724−15732], and titration of the R39Q mutant with *cis,cis*-muconate showed negative cooperativity [Harris, T. K., et al. (1999) *Biochemistry 38*, 12343−12357]. To test for anticooperativity during catalysis, 4-OT was titrated with equilibrium mixtures (≥81% product) of the reactive dicarboxylate or monocarboxylate intermediates, **2** or 2-hydroxy-2,4-pentadienoate (**4**), respectively, in three types of NMR experiments: two-dimensional $^{1}H-^{15}N$ HSQC titrations of backbone NH and of Arg NϵH resonances and one-dimensional ^{15}N NMR titrations of Arg Nϵ resonances. All titrations showed substoichiometric binding of the equilibrium mixtures to 3 ± 1 sites per hexamer with apparent dissociation constants comparable to the K_m values of the intermediates. Compound **4** also bound 1 order of magnitude less tightly at another site, suggesting negative cooperativity. Consistent with negative cooperativity, asymmetry of the resulting complexes at saturating levels of **2** and **4** is indicated by splitting of the backbone NH resonances of 11 residues and 10 residues of 4-OT, respectively. The dicarboxylate competitive inhibitor, (2*E*)-fluoromuconate (**5**), with a K_I of 45 ± 7 μM, also exhibited substoichiometric binding to 3 ± 1 sites per hexamer, with a K_D of 25 ± 18 μM, and splitting of the backbone NH resonance of L8. The monocarboxylate inhibitors (2*E*)- (**6**) and (2*Z*)-2-fluoro-2,4-pentadienoate (**7**) showed much weaker binding ($K_D = 3.1 \pm 1.3$ mM), as well as splitting of two and five backbone NH resonances, respectively, indicating asymmetry of the complexes. The Nϵ resonances of both Arg-11 and Arg-39 were shifted downfield, and that of Pro-1N was broadened by all ligands, consistent with the major catalytic roles of these residues. Structural pathways for the site−site interactions which result in negative cooperativity are proposed on the basis of the X-ray structures of free and affinity-labeled 4-OT. Selective resonance broadenings induced by the binding of inactive analogues and active intermediates indicate residues which may be mobilized during reversible ligand binding and during catalysis, respectively.

4-Oxalocrotonate tautomerase (4-OT)[1] catalyzes the conversion of unconjugated α-keto acids such as 2-oxo-4-hexenedioate (**1**, Scheme 1) to its conjugated isomer, 2-oxo-3-hexenedioate (**3**), via the dienolic intermediate, 2-hydroxymuconate (**2**), representing an important step in the bacterial degradation of aromatic hydrocarbons (*1*). A chemical mechanism for 4-OT has been proposed (Figure 1) (*2*), consistent with the X-ray structure (*3*, *4*), as well as with kinetic (*5*, *6*), NMR (*2*, *5*−*11*), mutagenesis (*2*, *7*−*9*), synthetic (*12*−*14*), and computational (*15*) studies, which can explain the $10^{7.3}$-fold rate acceleration produced by this enzyme (*2*). This mechanism involves the deprotonation of C-3 of the substrate by P1 acting as a general base, concerted with polarization of the C-2 carbonyl group by both R39″

Scheme 1

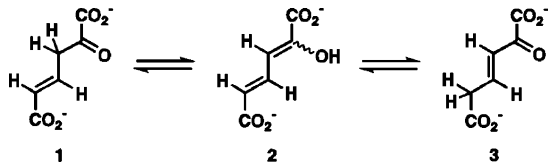

† This research was supported by National Institutes of Health Grants DK-28616 (to A.S.M.) and GM-41239 (to C.P.W.).

* To whom correspondence should be addressed. A.S.M.: telephone, (410) 955-2038; fax, (410) 955-5759; e-mail, mildvan@jhmi.edu. C.P.W.: telephone, (512) 471-6198; fax, (512) 232-2606; e-mail, whitman@mail.utexas.edu.

‡ The Johns Hopkins School of Medicine.

§ The University of Texas.

[1] Abbreviations: 2-FM, 2-fluoromuconate; (2*E*)-FPD, (2*E*)-fluoro-2,4-pentadienoate; (2*Z*)-FPD, (2*Z*)-fluoro-2,4-pentadienoate; 2-HM, 2-hydroxymuconate; 2-HPD, 2-hydroxy-2,4-pentadienoate; HSQC, heteronuclear single-quantum coherence; 4-OT, 4-oxalocrotonate tautomerase; P1(A), Pro-1 of the A subunit; SDS−PAGE, sodium dodecyl sulfate−polyacrylamide gel electrophoresis; TSP, sodium 3-(trimethylsilyl)propionate-2,2,3,3-d_4.

10.1021/bi0502590 CCC: $30.25
Published on Web 05/06/2005

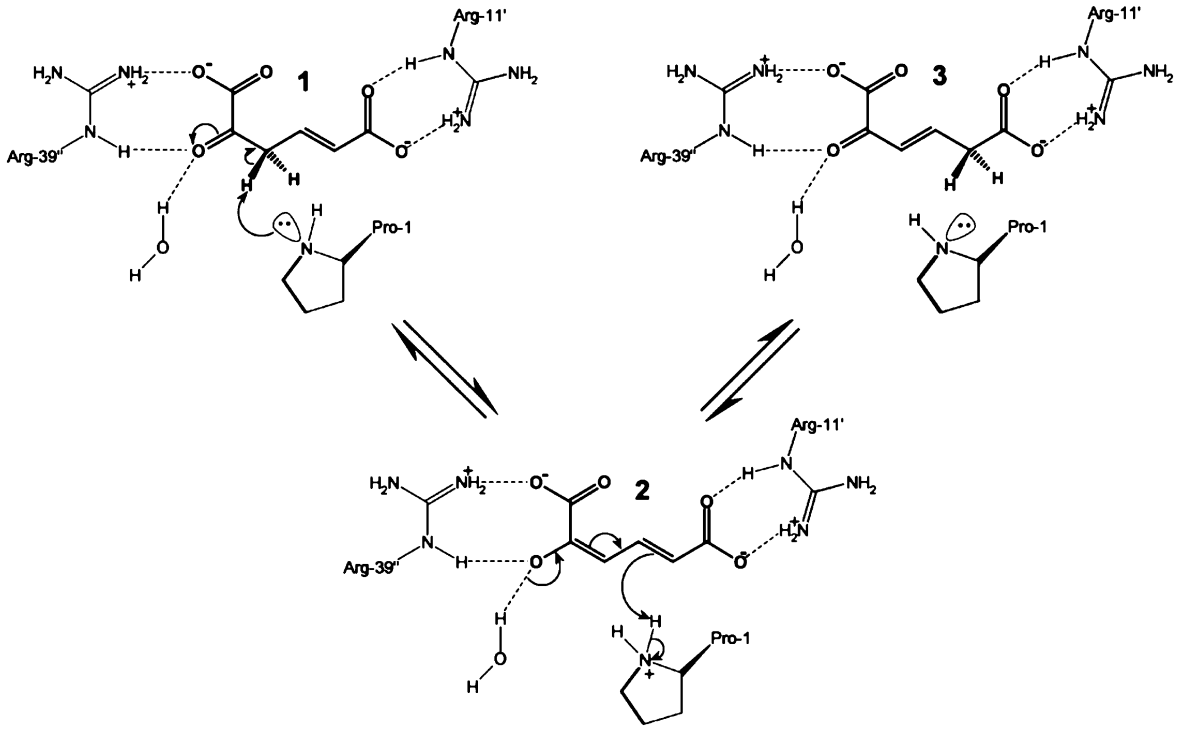

FIGURE 1: Reaction mechanism of 4-OT consistent with the results of kinetic, mutagenesis, NMR, synthetic, computational, and X-ray studies (*2*−*15*).

(from another subunit) and a fixed water molecule acting as Lewis acids, and/or hydrogen bond donors, to form an enolate intermediate. The catalytic residue, R11′ (from a third subunit), interacts with the 6-carboxylate group of the substrate and intermediate holding and orienting them for catalysis (*2*), which takes place in an otherwise hydrophobic active site, partially occluded by a β-hairpin (*8*). In the second step, P1 protonates C-5 of the intermediate which is concomitant with ketonization of the enolate.

The chemical mechanism of Figure 1 does not consider the possibility of site−site interaction, which is suggested by four observations. (i) The homohexameric 4-OT is a trimer of dimers in which each subunit contains only 62 residues (*3*, *4*) (Figure 2). (ii) The catalytic residues at each active site come from three different subunits (*4*). (iii) Enzyme inactivation by the affinity labels 3-bromopyruvate (*5*) and 2-oxo-3-pentynoate (*16*) shows half-site stoichiometry. (iv) Binding of the intermediate analogue *cis*,*cis*-muconate to the R39Q mutant of 4-OT shows negative cooperativity (*2*). These observations raise the possibility of negative cooperativity during catalytic turnover by 4-OT in which substrate binding at one site weakens substrate (and product) binding at another site, thereby minimizing product inhibition and promoting catalysis. Neither negative nor positive cooperativity has been detected in 4-OT by steady state kinetics, and no allosteric effectors have been found. Moreover, no asymmetry in the structure of the protein has been detected by NMR spectroscopy (*10*) or by X-ray crystallography (*3*, *4*). To test directly for negative cooperativity, and to determine which residues might become mobile during catalysis (*11*, *17*, *18*), we have carried out a series of NMR titration experiments of the enzyme with equilibrium mixtures of mono- and dicarboxylate substrates, intermediates (Scheme 2), and products, as well as with mono- and dicarboxylate intermediate analogues (Scheme 3). A preliminary abstract of this work has been published (*19*).

EXPERIMENTAL PROCEDURES

Materials. All reagents, enzymes, buffers, and solvents were obtained from Sigma Aldrich Chemical Co. (St. Louis, MO), unless otherwise noted. Amicon Ultra (10 000 MW cutoff) Millipore centrifugal filter devices were obtained from Fisher Scientific (Newark, DE). The syntheses of **2** and **4** are described in refs *20* and *21*, respectively. The syntheses of **5**−**7** are described in ref *22*. 2-Fluoromuconate consists of 93% of the (2*E*,4*E*) and 7% of the (2*Z*,4*E*) isomers (*22*), and is here termed (2*E*)-FM. The preparation of wild-type 4-OT and the construction, characterization, and purification of the R11A and R61A mutants, to ≥95% purity as judged by sodium dodecyl sulfate−polyacrylamide gel electrophoresis (SDS−PAGE), are described elsewhere (*2*).

General Methods. Protein was analyzed by Tris-glycine SDS−PAGE under denaturing conditions on 17.5% gels using a vertical gel electrophoresis apparatus obtained from Bio-Rad (Hercules, CA). Kinetic data were obtained using a Hewlett-Packard 8452A or an Agilent 8453 diode array spectrophotometer. Enzymatic assays were performed as described previously (*2*) following the increase in absorbance at 236 nm due to product formation. Protein concentrations were determined using the method of Waddell (*23*).

NMR Samples. Uniformly ^{15}N-labeled 4-OT and its mutants were prepared as described previously (*2*). Two sets of conditions were used in the NMR titration experiments, optimized for acquisition of either ^{1}H−^{15}N HSQC (selective for amide backbone NH or arginine NϵH resonances) or one-dimensional (1D) ^{15}N spectra focusing on the Arg Nϵ region. For the ^{1}H−^{15}N HSQC spectra, we found that pH 6.5 and 13 °C provided satisfactory conditions, with initial enzyme concentrations of either 4.0 or 0.4 mM subunits. The

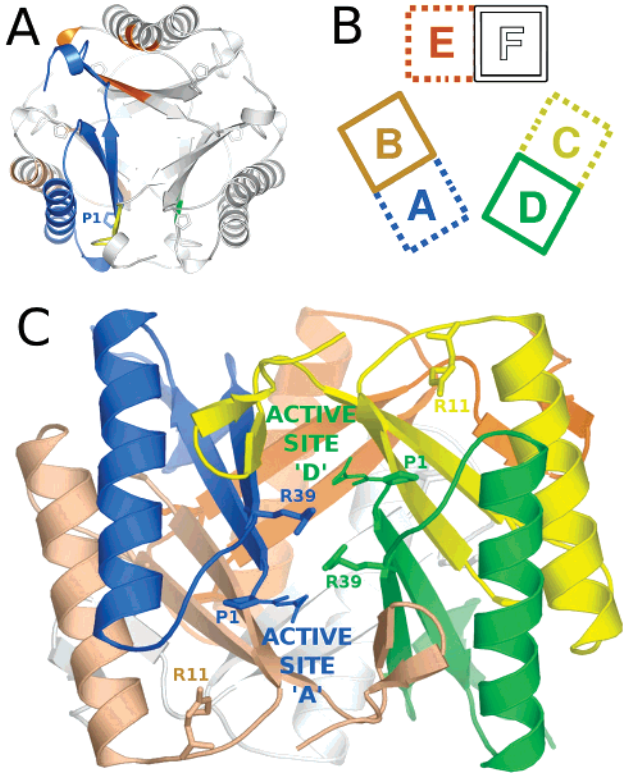

FIGURE 2: X-ray structure of affinity-labeled 4-OT (PDB entry 1BJP) (*4*). (A) "Top" view with the 3-fold axis perpendicular to the page. Only residues belonging to subunit A (blue) or in direct contact with it have been colored. (B) Diagram of the subunit arrangement in 4-OT, a trimer of dimers. Solid or dashed lines are used to represent active sites near or far from the reader, respectively. The following convention is used for coloring each subunit: blue for A, brown for B, yellow for C, green for D, orange for E, and white for F. (C) A 90° rotation from the view in panel A permitting visualization of active sites A and D, labeled according to the subunits providing the P1 residue. The affinity label 2-oxo-3(*E*)-pentenoate is covalently linked to P1 in thin stick representation.

Scheme 2

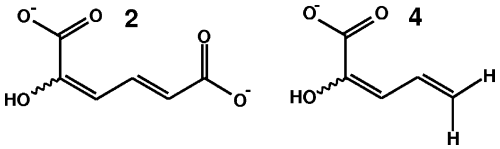

Scheme 3

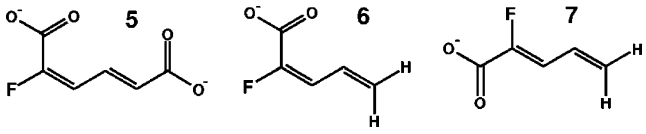

acquisition of well-resolved 1D Arg $^{15}N\epsilon$ spectra required an increase in the pH to 9.4 and the temperature to 42 °C with initial enzyme concentrations of 4.0 mM subunits. In all cases, the samples were prepared in 8 mM sodium phosphate buffer with 10% D_2O in a total volume of 0.35 mL, using Shigemi tubes (Shigemi, Inc., Allison Park, PA). High protein concentrations were used for the acquisition of high-quality 1D ^{15}N spectra and $^1H-^{15}N$ HSQC spectra in short time periods, as well as the accurate determination of the binding stoichiometries of substrates and analogues. Lower concentrations of enzyme were used to obtain more accurate dissociation constants. The intermediates or inhibitors were added in small volumes (0.5−10 μL) from stock solutions with appropriate concentrations (between 10 and 150 mM) preadjusted to the same pH as the protein sample. No pH changes were detected during the titrations. In titrations with kinetically active intermediates, a time period of 15 min was allowed after each addition for the complete equilibration of the substrate, intermediate, and product. From the steady state kinetic parameters of 4-OT (*2*), and the high enzyme concentrations used (0.4−4.0 mM subunits), complete equilibration (10 turnovers) of 2-HM and of 2-HPD would have occurred within 4 ms and 20 s, respectively.

NMR Titrations. NMR data were collected on Varian INOVA spectrometers at 500, 600, or 800 MHz, equipped with pulse field gradient units and using Varian probes, either 5 mm triple-resonance actively shielded *z*-gradient probes for the HSQC spectra or 5 mm broadband probes for the 1D ^{15}N NMR studies at 50.7 and 60.8 MHz. $^1H-^{15}N$ HSQC spectra selective for either amide backbone or arginine NϵH regions were acquired from uniformly ^{15}N-labeled samples of wild-type 4-OT and the R11A mutant. The ^{15}N chemical shifts were referenced to external liquid ammonia, and the proton chemical shifts were referenced to external TSP as described previously (*2*). The 1D ^{15}N NMR spectra were acquired without proton decoupling. The data were processed using NMRPipe (*24*) and analyzed with either NMRDraw (*24*) for the 1D spectra or Sparky (*25*) for the two-dimensional (2D) spectra. The dissociation constants were obtained by fitting the titration data, using nonlinear least-squares regression analysis, to either eq 1 (*2*), for changes in chemical shift, or eq 2, modified from eq 1, for fitting changes in intensity:

$$\Delta\delta_{obs} = (\Delta\delta_{max}/2E_t)\{K_D + L_t + E_t - [(K_D + L_t + E_t)^2 - 4L_tE_t]^{1/2}\} \quad (1)$$

$$I_{obs} = I_0 - (100/2E_t)\{K_D + L_t + E_t - [(K_D + L_t + E_t)^2 - 4L_tE_t]^{1/2}\} \quad (2)$$

where L_t is the total ligand concentration (substrate or inhibitor), E_t is the total binding site concentration, $\Delta\delta_{obs}$ is the observed chemical shift change, $\Delta\delta_{max}$ is the calculated chemical shift change at a saturating ligand concentration, I_{obs} is the observed peak intensity expressed as a percentage of the resonance intensity in the free enzyme, and I_0 is the measured peak intensity for the free enzyme. For E_t, all integral stoichiometries between 1 and 6 binding sites per 4-OT hexamer were considered. The best fit solutions for the ligand binding stoichiometries were chosen on the basis of two criteria: those which gave the lowest χ^2 values and those which gave the smallest relative errors in K_D. When these two criteria did not yield the same stoichiometry, the average stoichiometry between them was chosen, together with errors which covered the range. Because a fast-exchanging ligand may broaden resonances at several active sites within the time frame of observation, titrations involving changes in intensity, analyzed with eq 2, provide only lower limits to binding stoichiometries and dissociation constants.

RESULTS

$^1H-^{15}N$ HSQC NMR Titrations of 4-OT with 2-HM. The backbone $^1H-^{15}N$ HSQC spectral assignments for 4-OT were

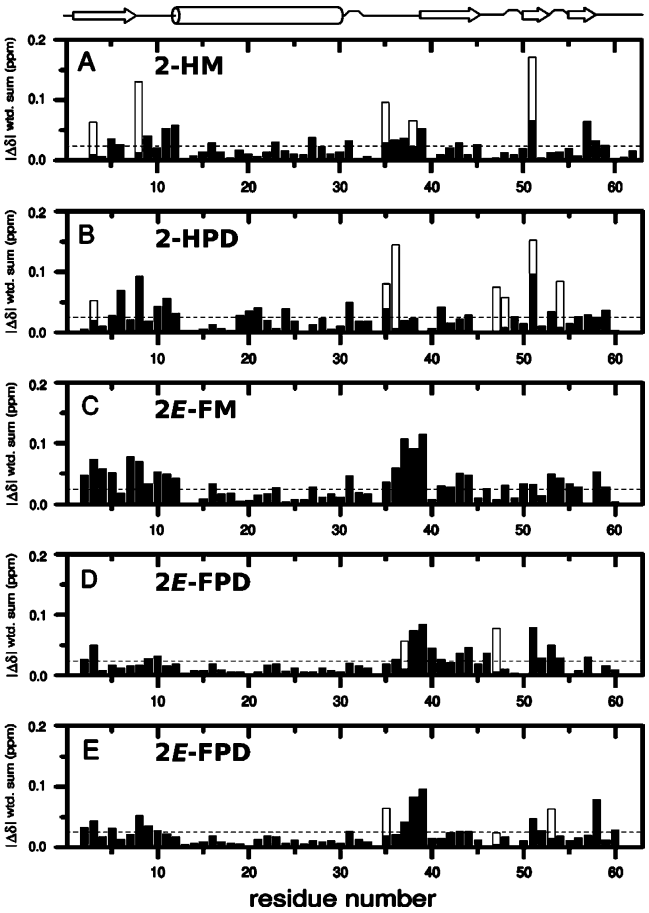

FIGURE 3: Weighted sum of changes in chemical shifts of backbone ^{15}N and NH resonances of 4-OT induced by binding of the indicated ligands. Chemical shift changes were weighted according to the backbone amide chemical shift dispersion in the ^{1}H (2.351 ppm) and ^{15}N (27.87 ppm) dimensions of the 4-OT spectrum. Resonances which were split at ligand saturation are represented by overlapping white and black bars. The dashed lines indicate the error level. The panels refer to saturation with (A) 2-HM, (B) 2-HPD, (C) (2*E*)-FM, (D) (2*E*)-FPD, and (E) (2*Z*)-FPD. The solution secondary structure of each subunit is shown above panel A (*10*).

previously reported (*10*). Titration of 4-OT with the intermediate 2-HM, which rapidly forms an equilibrium mixture of substrate, intermediate, and product in a 0.08/0.11/0.81 ratio in solution (*20*), produced a progressive overall broadening of several peaks followed by changes in chemical shifts and splittings of some of them (Figures 3A and 4A).[2] Beyond 4 equiv of 2-HM per subunit (or 24 equiv per hexamer), no further changes were observed in the spectra. The backbone NH resonances most broadened were those of residues L8, R39, A57, and S58, which at 0.4 equiv of 2-HM per subunit decreased their intensities to ~45%, for L8, R39, and A57, and to 19% in the case of S58. At saturating concentrations of 2HM (>4 equiv per subunit), the backbone NH signals of A3, I7, L8, R39, G51, G54, A57, S58, and V60 became very broad. In addition, as indicated in Figure 3A, 22 backbone NH resonances widely distributed throughout the protein showed significant changes in chemical shifts greater than the noise level. Nine residues which showed shifts of more than twice the noise level, when mapped onto the protein structure (Figure 4A), are seen to surround the active site, consistent with active site binding.

[2] No changes in pH occurred during the titrations.

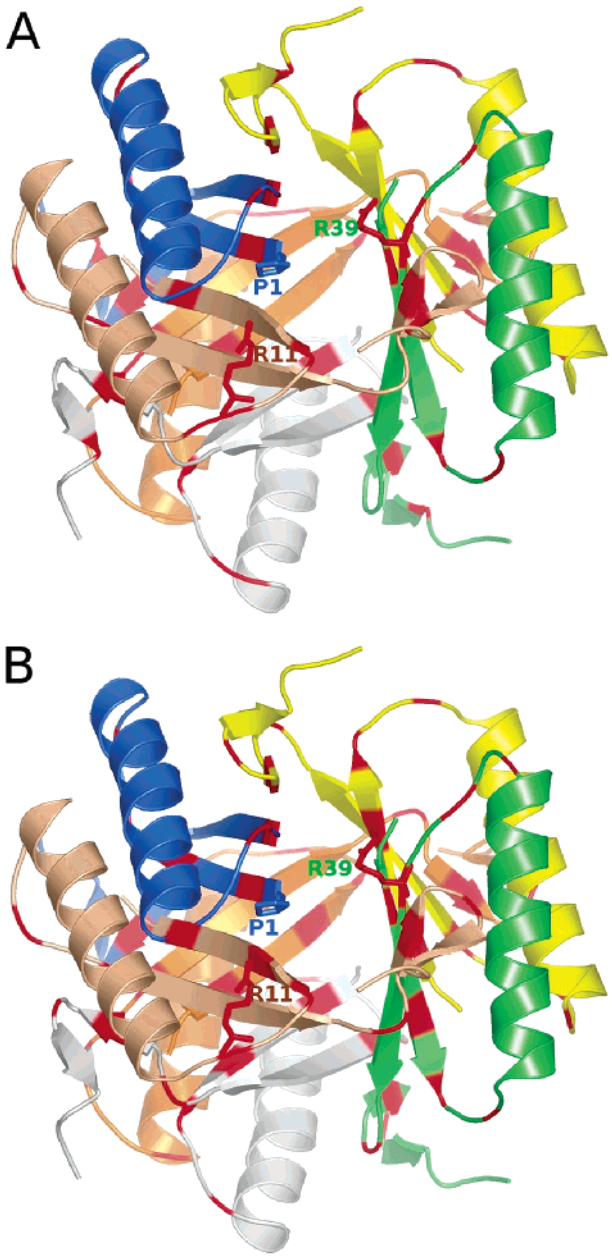

FIGURE 4: Mapping of the residues with backbone ^{15}N and NH chemical shift changes greater than twice the error onto the X-ray structure of affinity-labeled 4-OT (red residues). The enzyme was saturated with intermediates 2-HM (A) and 2-HPD (B). For clarity, the protein orientation has been chosen to show a direct view of active site A, defined as containing P1 of the A subunit. The color coding for each subunit is given in the legend of Figure 2.

As indicated by the pairs of black and white bars in Figure 3A, and exemplified in panels A and B of Figure 5, the backbone resonances of 10 residues throughout the protein were split in the complex, indicating that an asymmetry was induced in the protein upon saturation with a reactive intermediate. Table 1 lists the magnitudes of the splittings and the distances of the residues with split signals from P1 N in the active site as found in the X-ray structure of the affinity-labeled enzyme (PDB entry 1BJP) (*4*). Splittings of resonances were not found for residues in the α-helix or in *β*-strand 2 (Figure 3A) which are on the outside of each dimer, and farther from the active sites.

The changes in chemical shift (Δδ) as a function of the total ligand concentration in the 2-HM equilibrium mixture

Table 1: Split Resonances at the End of the Titrations with Reactive Intermediates 2-HM (**2**) and 2-HPD (**4**)

intermediate	residue	interaction with substrate[a]	distance from P1 N[b] (Å)	Δδ (ppm) ^{15}N[c]	Δδ (ppm) ^{1}H[c]
2-HM (**2**)	A3	>2nd shell	6.8	0.82	0.118
	L8	contact	6.2	1.0	0.24
	R11	contact	11.8 (8.2 for Nη)	0.2	0.09
	L35	>2nd shell	9.0	0.1	0.187
	T36	>2nd shell	9.0	2.7	0.31
	S37	contact	6.7 (4.0 for O)	1.3	0.08
	V38	2nd shell	5.2	0.9	0.148
	R39	contact	5.6	1.0 (Nε)	–
	G51	>2nd shell	11.0	0.21	0.227
	G53	>2nd shell	9.4	0.05	0.176
	S58	>2nd shell	13.2	0.4	0.21
2-HPD (**4**)	A3	>2nd shell	6.8	0.63	0.094
	L35	>2nd shell	9.0	0.5	0.062
	T36	>2nd shell	9.0	1.4	0.216
	S37	contact	6.7 (4.0 for O)	0.60	0.136
	R39	contact	5.6	0.8 (Nε)	–
	K47	>2nd shell	12.6	0.35	0.148
	G48	>2nd shell	14.2	1.14	0.081
	G51	>2nd shell	11.0	1.10	0.097
	G54	>2nd shell	11.0	0.68	0.197
	R61	contact	11.8 (8.2 for Nε)	0.05 (Nε)	0.07 (NεH)

[a] Based on modeling of the substrate into the active site in X-ray structure 1BJP. [b] All distances are to P1 N from the backbone N of the residue in X-ray structure 1BJP, except where indicated. [c] The resonances are from the backbone NH group, except where indicated.

could not be fit to eq 1 with a binding stoichiometry of 6 binding sites per hexamer. Consideration of all integral stoichiometries from 1 to 6 revealed that substoichiometric binding was taking place. An example of the curve fitting is shown in Figure 6A for Δδ of the resonance of S12 in the ^{15}N dimension, where theoretical curves were calculated for 1−6 binding sites per hexamer. From the plots, it appears that three or four binding sites per hexamer provide the best fit to the titration data, which represents the average stoichiometry obtained by the criteria of minimizing both χ^2 and the relative error in K_D. The data from the backbone HSQC titrations with the highest signal-to-noise ratio, monitoring G10 N, S12 N, S12 NH, K16 NH, and E17 NH, yielded an average stoichiometry of 3.0 ± 1.2 sites per hexamer and an apparent dissociation constant (K_D^{app}) of 0.79 ± 0.43 mM (Table 2).

Arg Nε^{1}H−^{15}N HSQC Titrations of 4-OT with 2-HM. The previously assigned Arg HSQC spectrum of wild-type 4-OT showed only five of the six potential Arg NεH resonances (R11, R21, R29, R61, and R62), but not R39 (*2*). The addition of 2-HM most affected the R11 NεH signal, which continuously broadened, almost to disappearance, and shifted downfield by 0.08 ppm in the ^{1}H dimension and by 0.35 ppm in the ^{15}N dimension (Figure 6B). This broadened signal was absent in the 2-HM complex of the R11A mutant, confirming its assignment to R11 NεH. R29 NεH and R61 NεH showed much smaller changes in chemical shifts ($\Delta\delta \leq 0.05$ ppm for ^{1}H and $\Delta\delta \leq 0.2$ ppm for ^{15}N), while no effects were observed on the signals of R21 and R62. The decreasing intensity of the resonance of R11 NεH with an increasing concentration of 2-HM was fit to eq 2, yielding a lower-limit stoichiometry of ≥2.0 ± 1.0 sites per hexamer and a lower limit K_D^{app} of ≥0.11 ± 0.04 mM (Table 2).

1D ^{15}N NMR Titration of 4-OT with 2-HM. This set of experiments was performed at 42 °C and pH 9.4 for optimum signal-to-noise ratio and resolution of the Arg Nε resonances. Under these conditions, the enzyme is highly active[3] with a k_{cat} of 4550 s^{-1} and a K_m for 2-HM of 69 μM, and the previously assigned Nε resonances of all six arginine residues of 4-OT were detected (*2*). Upon addition of 2-HM, the signals most affected were those of R11 and R39, both of which shifted downfield and broadened, while the weak resonance of P1 broadened into the baseline during the titration. The continuously changing chemical shifts of the R11 Nε resonance could be accurately measured and analyzed (Figure 6C). Following the criteria of minimum χ^2 and minimum relative error of the K_D^{app}, the stoichiometry was 3.0 ± 1.0 binding sites per hexamer with a K_D^{app} of 0.55 ± 0.12 mM, in agreement with the results of the other titration experiments (Table 2). In the case of R39 Nε, the broadening was greater, with the signal disappearing into the noise beyond 2 equiv of 2-HM per subunit, precluding quantitative analysis of these data. Qualitatively, however, the broadening of the R39 Nε resonance was accompanied by splitting of the peak into two signals (Table 1), indicative of a heterogeneous environment for R39 Nε under conditions of partial and maximal ligand occupancy.

^{1}H−^{15}N NMR Titrations with 2-HM at a Lower 4-OT Concentration. Although high protein concentrations are often necessary in obtaining precise and accurate binding stoichiometries, they are generally unsuitable for measuring low K_D values (*26*), in some cases due to protein aggregation. Indeed, the K_D^{app} values of the 2-HM equilibrium mixture obtained at 4.0 mM 4-OT subunits (0.79 ± 0.43 mM, Table 2) are slightly greater than the reported K_M value of 0.28 mM for 2-HM (*5*). To explore the possibility that the protein concentration might be influencing the K_D^{app} values, we repeated the HSQC titrations with 2-HM, using a 10-fold lower protein concentration (0.4 mM in 4-OT subunits) but under otherwise identical conditions. Analysis of the chemical shift changes of the backbone NH resonances of G10, R11, and V60 with eq 1 yielded values of K_D^{app} of 0.24 ± 0.18 mM (Figure 7A and Table 2), comparable to the K_m. However, because of the small $\Delta\delta_{max}$, the fits to eq 1 were

[3] S. G. Miller and C. P. Whitman, unpublished observations, 2004.

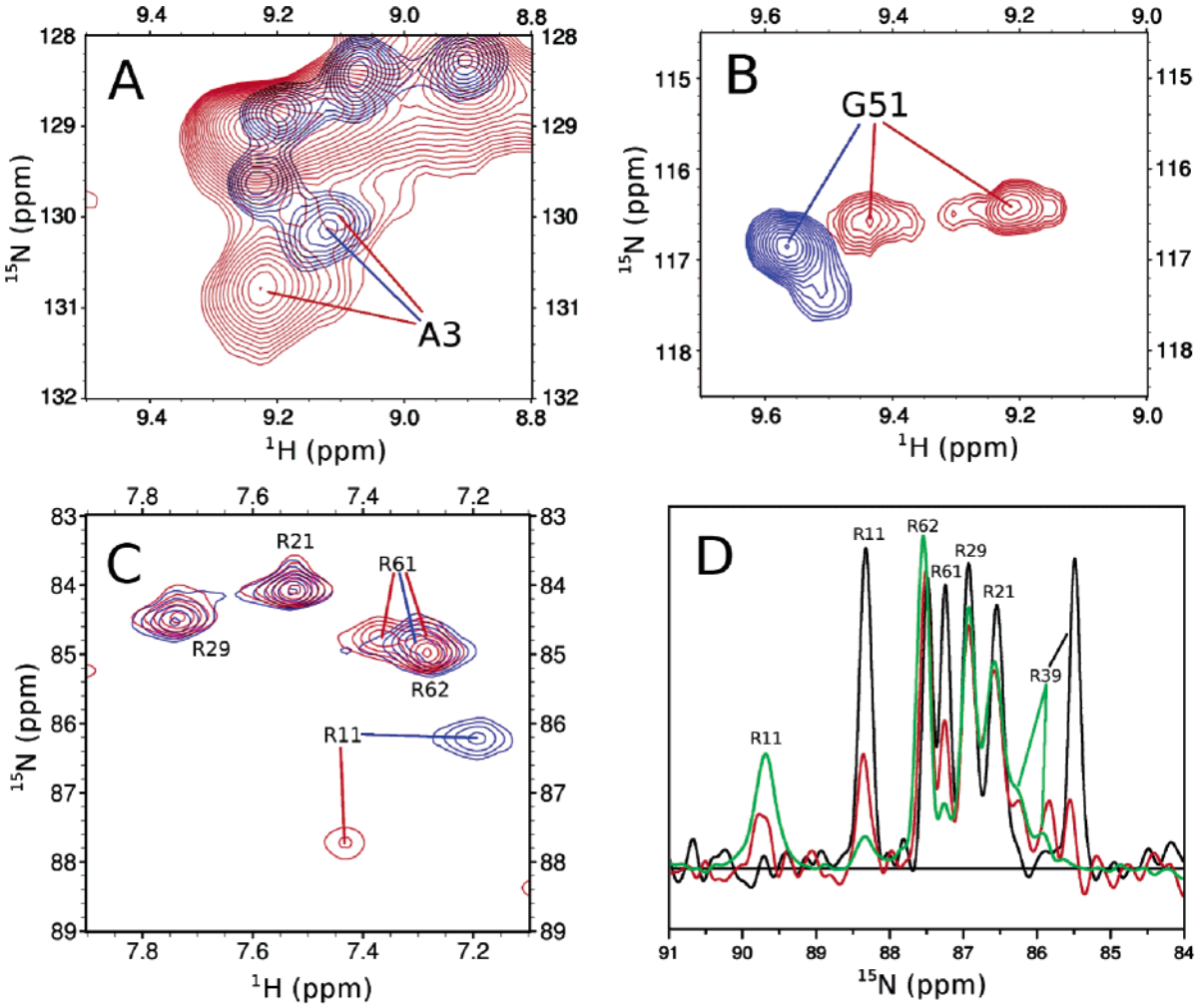

FIGURE 5: Examples of resonances showing splitting at the end of titrations: (A) A3 NH and (B) G51 NH, from the HSQC spectra of free 4-OT (blue contours) and 4-OT saturated with 2-HM (red contours). (C) Arg NϵH HSQC spectra of free 4-OT (blue contours) and 4-OT saturated with 2-HPD (red contours). (D) 1D ^{15}N NMR spectra of free 4-OT (black line) and 4-OT with ~0.9 (red line) and ~2.2 (green line) equiv of 2-HPD. The 4-OT concentration was 6.5 mM in subunits.

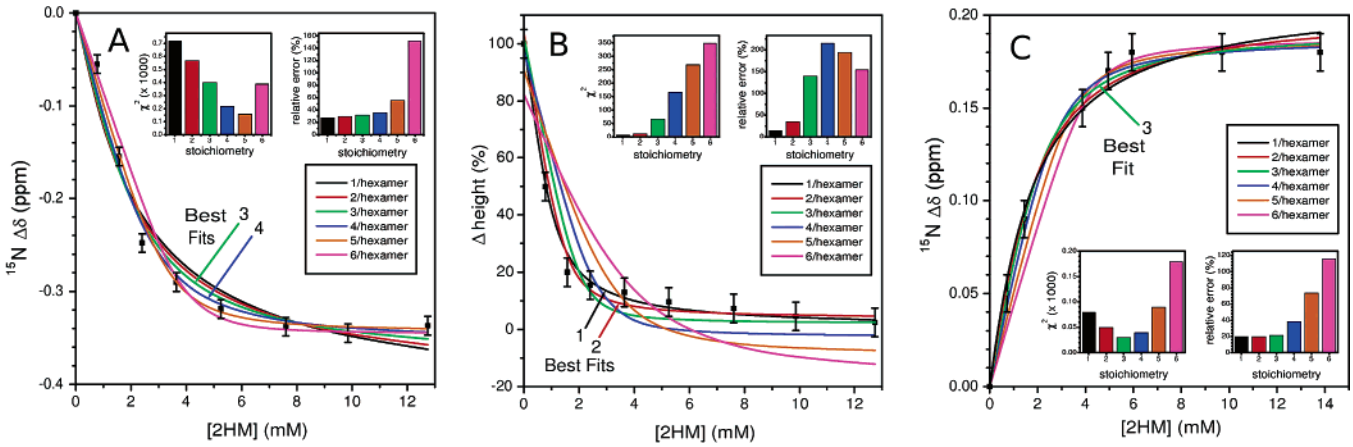

FIGURE 6: Examples of curve fitting from titrations of 4-OT with 2-HM: (A) backbone NH of S12, (B) NϵH of R11, and (C) Nϵ of R11 from 1D experiments. The inset graphs show the χ^2 and relative error values obtained for each case, as functions of the assumed stoichiometry of ligand binding sites per hexamer.

insensitive to the binding stoichiometry. At the lower protein concentration, the backbone NH resonances of L8, R39, A57, and S58 decreased in intensity with increasing 2-HM concentrations. Analysis of the titration data of R39 and S58 with eq 2 yielded a lower-limit K_D^{app} value of $\geq 42 \pm 22$ μM and a lower-limit stoichiometry of $\geq 1.5 \pm 0.5$ sites per hexamer. This low K_D^{app} value is 6.7-fold lower than the K_M and may result from exchange among several conformational states, which could rapidly attenuate the resonances before maximal occupancy is achieved.

^{1}H−^{15}N HSQC NMR Titrations of 4-OT with 2-HPD. At equilibrium, the monocarboxylate intermediate 2-HPD is

Table 2: K_D^{app} Values and Stoichiometries Obtained from the Titrations of 4-OT with Reactive Intermediates 2-HM (**2**) and 2-HPD (**4**) under the Indicated Conditions[a]

intermediate	conditions	resonances	data fit	K_D^{app} (mM)	stoichiometry (no. of active sites per hexamer)
2-HM (**2**)	pH 6.5 and 13 °C	N (G10, S12), NH (S12, K16, E17)	$\Delta\delta_{obs}$	0.79 ± 0.43	3.0 ± 1.2
		NεH (R11)	I_{obs}	$\geq 0.11 \pm 0.04$	$\geq 2.0 \pm 1.0$
	pH 6.5 and 13 °C[b]	NH (G10, R11, V60)	$\Delta\delta_{obs}$	0.24 ± 0.18	undefined
		NH (R39, S58)	I_{obs}	$\geq 0.042 \pm 0.022$	$\geq 1.5 \pm 0.5$
	pH 9.4 and 42 °C	Nε (R11)	$\Delta\delta_{obs}$	0.55 ± 0.12	3.0 ± 1.0
2-HPD (**4**)	pH 6.5 and 13 °C	NH (H49)	$\Delta\delta_{obs}$	0.59 ± 0.20	2.0 ± 1.0
		NH (I41)	$\Delta\delta_{obs}$	5.1 ± 0.7	undefined
		NH (L8, V38, R39, M45, G51, A57)	I_{obs}	$\geq 0.97 \pm 0.41$	$\geq 2.2 \pm 1.0$
		NεH (R11)	I_{obs}	$\geq 0.80 \pm 0.12$	$\geq 4.0 \pm 1.0$
	pH 9.4 and 42 °C	Nε (R11, R39)	I_{obs}	$\geq 1.4 \pm 0.5$	$\geq 4.0 \pm 1.0$

[a] The enzyme concentration was 4.0 mM in subunits, except where indicated. [b] Tenfold lower enzyme concentration, 0.4 mM in subunits.

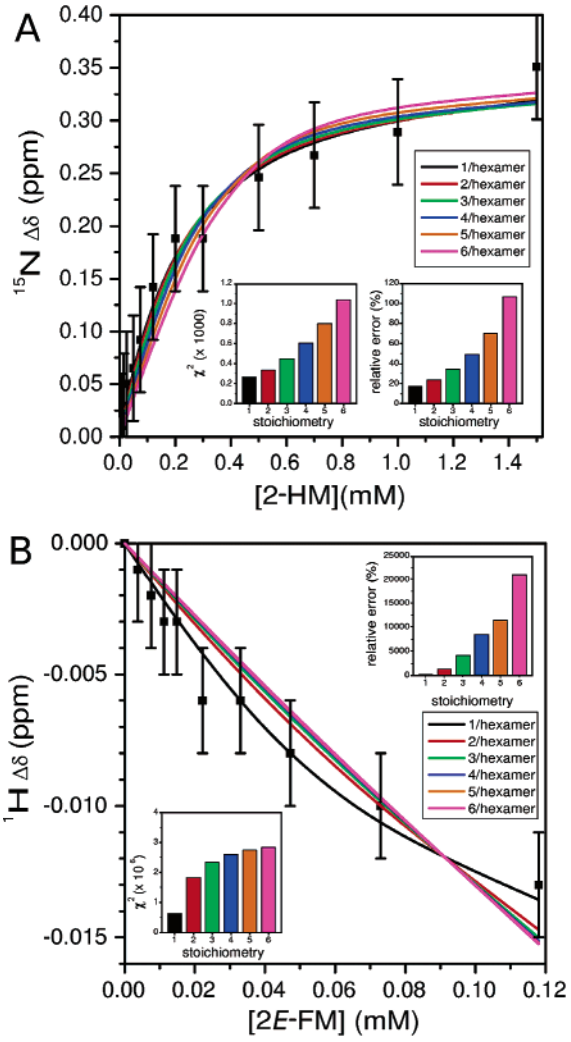

FIGURE 7: HSQC titration curves obtained at a low protein concentration (0.4 mM subunits) for (A) R11 Nε titrated with 2-HM and (B) T36 NH titrated with (2*E*)-FM. The inset graphs show the χ^2 and relative error as functions of the assumed binding stoichiometry.

predominantly (>99%) converted to the product, 2-oxo-3(*E*)-pentenoate (*21*). Titrations of 4-OT with 2-HPD (**4**) were carried out under the same conditions that were used with 2-HM. The ^{1}H and ^{15}N chemical shift changes in 4-OT upon saturation with 2-HPD (21 equiv per hexamer) are shown in Figure 3B, with pairs of black and white bars representing eight backbone resonances that exhibited splitting, indicative of asymmetry in the 2-HPD complex of 4-OT (Table 1). The backbone NH resonance of R39 showed splitting in the course of the titration and disappeared beyond 2.6 equiv of 2-HPD per subunit. Of the 54 peaks analyzed in the titration, 25, located throughout the protein, exhibited combined ^{15}N and NH chemical shift changes greater than the error (Figure 3B). Mapping the 11 residues which showed backbone chemical shifts of more than twice the noise level shows that they surround the active site (Figure 4B).

The only chemical shifts that could be continuously followed throughout the titration were those of H49 NH and I41 NH. Fitting the observed $\Delta\delta$(NH) for H49 NH to eq 1 yielded a stoichiometry of 2.0 ± 1.0 binding sites per hexamer and a K_D^{app} of 0.59 ± 0.20 mM, by the criteria of minimizing both χ^2 and the relative error in K_D (Figure 8A and Table 2). The same analysis of I41 NH showed a 1 order of magnitude weaker binding with a K_D of 5.1 ± 0.7 mM (Figure 8B and Table 2), suggesting negative cooperativity between binding sites. Because of the lower affinity for the ligand at this site, the binding stoichiometry was undefined.

The most notable changes were not in chemical shifts but in the strong broadening (most of them to disappearance) displayed by several amide resonances, including those of L8, V38, R39, M45, G51, and A57. The decreasing intensities of these amide backbone resonances were analyzed by fitting to eq 2 as exemplified for V38 NH in Figure 8C. After the best values were selected using the criteria of the minimum relative error in K_D^{app} and χ^2, an average lower limit stoichiometry of $\geq 2.2 \pm 1.0$ binding sites per hexamer and a lower-limit K_D^{app} value of $\geq 0.97 \pm 0.41$ mM were obtained (Table 2).

Arg NεH ^{1}H−^{15}N HSQC Titrations of 4-OT with 2-HPD. The Arg HSQC experiments showed no continuous changes in chemical shifts, but progressive decreases in intensity of the R11 NεH and R61 NεH resonances, with little or no effect on the other observed NεH signals (R21, R29, and R62 NεH). The disappearance of R11 was accompanied by the appearance of a new downfield peak near the position found for R11 NεH during the 2-HM titration, and with the same low intensity. Both signals were absent in the 2-HPD complex of the R11A mutant, confirming their assignment to R11 NεH. Fitting these data to eq 2 (not shown) yielded a lower-limit stoichiometry of $\geq 4.0 \pm 1.0$ sites per hexamer for 2-HPD with a lower-limit K_D^{app} of $\geq 0.80 \pm 0.12$ mM (Table 2).

Similarly, the decreasing intensity of the resonance of R61 was accompanied by the appearance of a second peak at

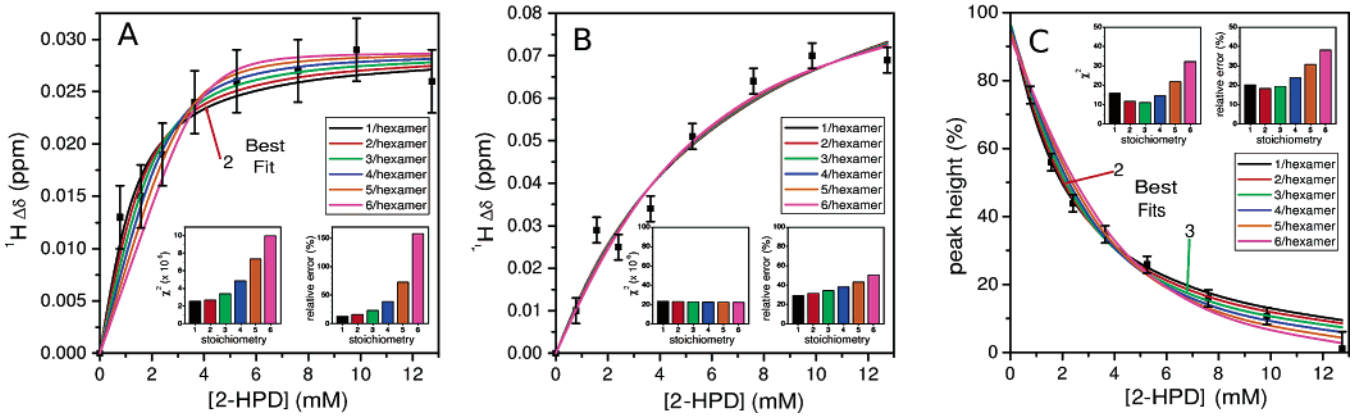

FIGURE 8: Backbone HSQC titration curves obtained with intermediate 2-HPD for (A) Δδ of H49 NH, (B) Δδ of I41 NH, and (C) the peak height of the V38 NH resonance. The inset graphs show the χ^2 and relative error as functions of the assumed binding stoichiometry.

saturation with the same $\delta(^{15}N)$ but with an 0.08 ppm downfield $\delta(^1H)$, suggesting asymmetry in the environment of R61 NϵH in the 2-HPD complex (Figure 5C and Table 1). Because of the partially overlapping signals of R61 NϵH and R62 NϵH, accurate stoichiometry or K_D^{app} values could not be computed from the changes in the R61 signal. However, it is noteworthy that kinetic studies showed no effects of the R61A mutation on k_{cat} or K_m using either 2-HM (*2*) or 2-HPD[3] as the substrate.

1D ^{15}N NMR Titration of 4-OT with 2-HPD. At pH 9.4 and 42 °C, conditions differing from those of the HSQC experiments, the 1D ^{15}Nϵ resonances of R11, R39, and R61 progressively decreased in intensity with increasing levels of intermediate 2-HPD, with only one new broader peak appearing downfield at 89.7 ppm at saturation (Figure 5D). This downfield resonance is assigned to R11 Nϵ on the basis of its absence in the 2-HPD complex of the R11A mutant. Like the backbone NH signal of R39 in the HSQC spectrum, the R39 Nϵ resonance downshifted, broadened, and split in the course of the titration, but with Nϵ, the splitting was also detected at saturation (Figure 5D and Table 1). The titrations monitoring the intensities of the R11 Nϵ and R39 Nϵ resonances could be fit with eq 2, yielding a stoichiometry of $\geq 4.0 \pm 1.0$ sites per hexamer and a K_D^{app} of $\geq 1.4 \pm 0.5$ mM under these different conditions (Table 2). Because of overlap, the R61 Nϵ resonance could not be accurately analyzed. The weak ^{15}N resonance of P1, the catalytic base, was broadened beyond detection during the titration.

NMR Titrations of 4-OT with the Dicarboxylate Inhibitor 2E-FM. Backbone and Arg NϵH HSQC titrations of 4.0 mM 4-OT subunits were carried out with the dicarboxylate competitive inhibitor (2*E*)-FM (**5**) under the same conditions that were used with the substrates. When ~1 equiv per hexamer of (2*E*)-FM was added, five of the backbone NH resonances, those of V38, G51, G53, A57, and S58, broadened into the baseline, while smaller broadenings of I7 and S37 were found. Also, in the initial stage of the titration, split peaks were observed for the backbone NH resonances of A3, L8, and G54, suggesting two states, exchanging slowly, at a rate of less than 220 s^{-1}, as estimated from the splitting. As the titration progressed, new peaks appeared near the peaks that had disappeared, and the split signals of A3 and G54 became single peaks, while the L8 signal remained split at saturation with (2*E*)-FM, suggesting an asymmetric environment for this residue (Table 3).

Table 3: Split Resonances at the End of the Titrations with the Intermediate Analogue Inhibitors

inhibitor	residue	interaction with inhibitor[a]	distance from P1 N[b] (Å)	Δδ (ppm) ^{15}N[c]	Δδ (ppm) ^{1}H[c]
(2*E*)-FM (**5**)	L8	contact	6.2	1.50	0.166
(2*E*)-FPD (**6**)	S37	contact	6.7 (4.0 for O)	0.77	0.054
	K47	>2nd shell	12.6	0.35	0.147
(2*Z*)-FPD (**7**)	A3	>2nd shell	6.8	0.2	0.135
	L35	>2nd shell	9.0	0.2	0.126
	S37	contact	6.7 (4.0 for O)	0.33	0.052
	K47	>2nd shell	12.6	0.3	0.147
	G53	>2nd shell	9.4	0.17	0.108

[a] Based on modeling of inhibitor into the active site in X-ray structure 1BJP. [b] All distances are to P1 N from the backbone N of the residue in X-ray structure 1BJP, except where indicated. [c] The resonances are from the backbone NH group, except where indicated.

Overall, 32 residues exhibited changes in chemical shifts beyond experimental error (Figure 3C). The changes in chemical shift as a function of (2*E*)-FM concentration for the backbone NH signals of G10, R11, L31, L35, S37, V38, and R39, when fit to eq 1, yielded an average stoichiometry of 2.8 ± 0.4 sites per hexamer and a K_D of 0.30 ± 0.12 mM (Table 4).

In the Arg NϵH titrations, the signals most affected were those of R11 and to a lesser extent R61, which showed continuous changes in chemical shifts with increasing ligand concentrations. Upon saturation with (2*E*)-FM, the total change in chemical shift of the R11 NϵH resonance was 0.340 ppm downfield in the ^{1}H dimension and 0.69 ppm downfield in the ^{15}N dimension. For R61 NϵH, Δδ was 0.062 ppm downfield in the ^{1}H dimension and 0.33 ppm *upfield* in the ^{15}N dimension. Fitting the large changes in the ^{1}H chemical shift of the R11 NϵH resonance to eq 1 yielded a stoichiometry of 3.0 ± 1.0 sites per hexamer and a K_D of 0.31 ± 0.05 mM (Table 4). These K_D values, obtained at pH 6.5 and 13 °C, were 6.9-fold greater than the kinetically determined K_I value of 45 ± 7 μM obtained under somewhat different conditions (pH 7.3 and 22 °C) (*19*). (See below.)

1D ^{15}N titrations with (2*E*)-FM were carried out at pH 9.4 and 42 °C to optimize sensitivity and resolution. The Nϵ resonances of R11 and R39 were shifted downfield by 0.4 and 1.4 ppm, respectively. In the case of R39, the change was accompanied by broadening. When the data were fit to eq 1, a stoichiometry of 3 sites per hexamer was found to give slightly better results than the other alternatives, but

Table 4: K_D Values Obtained from the Titrations of 4-OT with Intermediate Analogue Inhibitors (2*E*)-FM (**5**), (2*E*)-FPD (**7**), and (2*Z*)-HPD (**8**) under the Indicated Conditions[a]

inhibitor	conditions	resonances	data fit	K_D (mM)	stoichiometry (no. of active sites per hexamer)
(2*E*)-FM (**5**)	pH 6.5 and 13 °C	N (G10, R11, L35, S37, V38, R39), NH (G10, L31, S37)	$\Delta\delta_{obs}$	0.30 ± 0.12	2.8 ± 0.4
		NϵH (R11)	$\Delta\delta_{obs}$	0.31 ± 0.05	3.0 ± 1.0
	pH 7.3 and 22 °C[b]	NH (T36)	$\Delta\delta_{obs}$	$25 \pm 18 \times 10^{-3}$	1.5 ± 0.5
		NH (I2, I52, G53, A57, S58)	I_{obs}	$(\geq 6.5 \pm 4.5) \times 10^{-3}$	$\geq 2.2 \pm 1.3$
	pH 9.4 and 42 °C	Nϵ (R11)	$\Delta\delta_{obs}$	2.35 ± 0.94	3.0 ± 1.0
(2*E*)-FPD (**6**)	pH 6.5 and 13 °C	N (R11, V38, G51), NϵH (R11)	$\Delta\delta_{obs}$	3.0 ± 1.5	undefined
	pH 9.4 and 42 °C	Nϵ (R11, R39)	$\Delta\delta_{obs}$	8.5 ± 2.1	undefined
(2*Z*)-FPD (**7**)	pH 6.5 and 13 °C	N (R11, L35, G51), NH (L8), NϵH (R11)	$\Delta\delta_{obs}$	3.2 ± 1.2	undefined
	pH 9.4 and 42 °C	Nϵ (R11, R39)	$\Delta\delta_{obs}$	9.4 ± 2.8	undefined

[a] The enzyme concentration was 4.0 mM in subunits, except where indicated. [b] Tenfold lower enzyme concentration, 0.4 mM in subunits.

the differences among them were small (Table 4). The average K_D value computed from the data (2.35 ± 0.94 mM) suggested that the conditions required for monitoring the 1D NMR titration with (2*E*)-FM were not optimal for binding to 4-OT (see below). As found with the substrate titrations, the ^{15}N resonance of P1 became broadened beyond detection during the titration.

$^1H-^{15}N$ NMR Titrations with 2E-FM at a Lower 4-OT Concentration. For a proper comparison with the K_I of 45 ± 7 μM obtained kinetically with the dicarboxylate inhibitor (2*E*)-FM (*22*), 0.4 mM subunits of 4-OT were titrated with (2*E*)-FM under conditions of the kinetic experiment at pH 7.3 and 22 °C. A single resonance, the backbone NH resonance of T36, exhibited a small but continuous upfield shift with a $\Delta\delta_{max}$ of -0.021 ppm, with several titration points in the sensitive curvilinear region. Fitting the data with eq 1 yielded a K_D of 25 ± 18 μM (Figure 7B and Table 4), comparable to the K_I, and a low binding stoichiometry between 1 and 2 sites per hexamer.

In the course of the titration, nine backbone NH resonances did not shift but decreased in intensity and disappeared (I2, A3, I7, R39, G51, I52, G53, A57, and S58). The heights of five of these resonances which were well-resolved (I2, I52, G53, A57, and S58) were fit to eq 2, yielding an average lower-limit stoichiometry of $\geq 2.2 \pm 1.3$ sites per hexamer and an average lower-limit K_D value of $\geq 6.5 \pm 4.5$ μM (Table 4). The lower-limit K_D so obtained is 7-fold lower than the K_I value, which may result from ligand-induced exchange among multiple conformations, efficiently broadening the observed resonances.

HSQC NMR Titrations of 4-OT with Monocarboxylate Inhibitors. Titrations with the monocarboxylic inhibitors (2*E*)-FPD and (2*Z*)-FPD were performed under conditions identical to those used with (2*E*)-FM, namely, 4.0 mM enzyme subunits, pH 6.5, and 13 °C. With (2*E*)-FPD, 13 backbone NH resonances were severely broadened, those of A3, Q4, I5, H6, L8, R39, M45, G48, G51, G53, G54, A57, and S58. Of the 17 residues that showed changes in backbone NH chemical shifts (Figure 3D), only the resonances of R11, V38, and G51 showed changes sufficiently large to be accurately analyzed. In the Arg HSQC titration, the R11 NϵH signal was the only one significantly affected, showing continuous changes in chemical shift, with an overall $\Delta\delta_{max}$ at saturation of 0.166 ppm downfield in the ^1H dimension. The average K_D value for (2*E*)-HPD obtained from the chemical shift changes of these four resonances using eq 1 was 3.0 ± 1.5 mM (Table 4). Because of the low affinity, the binding stoichiometry of (2*E*)-FPD was not well defined. In addition, two backbone NH resonances, those of S37 and K47, showed splitting upon ligand saturation, indicating asymmetry in the (2*E*)-FPD complex (Table 3).

HSQC titrations with (2*Z*)-FPD yielded results similar to those found with (2*E*)-FPD for both the backbone NH (Figure 3E) and Arg NϵH signals, with the exception of the backbone NH signals of E44 and L8. The NH resonance of E44 was only slightly broadened, and the NH resonance of L8 was not broadened, but continuously shifted to 0.066 ppm downfield in the ^1H dimension and 0.62 ppm downfield in the ^{15}N dimension at saturation. The average K_D value obtained for the titration with (2*Z*)-FPD was 3.2 ± 1.2 mM (Table 4). Again, because of the low affinity, the binding stoichiometry of (2*Z*)-FPD was not well defined. Saturating levels of (2*Z*)-FPD produced splitting of five backbone resonances, including those of S37 and K47 found with 2-HPD, indicating structural asymmetry in the (2*Z*)-FPD complex (Table 3).

At pH 9.4 and 42 °C, 1D ^{15}N titrations with the monocarboxylate inhibitors showed the Nϵ resonances of both R11 and R39 to continuously shift downfield, yielding from eq 1 average K_D values of 8.5 ± 2.1 mM for (2*E*)-FPD and 9.4 ± 2.8 mM for (2*Z*)-FPD (Table 4). With both monocarboxylate isomers, the binding constants were weaker than with the dicarboxylate (2*E*)-FM, and consequently, the binding stoichiometries were undefined. As with the other active site ligands, the weak ^{15}N resonance of P1 became broadened beyond detection during the titrations.

DISCUSSION

Both negative cooperativity and its limiting case, half-of-the-sites binding stoichiometry, are generally accompanied by ligand-induced structural asymmetry in multisubunit enzymes (*27*). Previous studies of 4-OT detected half-of-the-sites stoichiometry in the inactivation of this enzyme by the affinity labels 3-bromopyruvate (*5*) and 2-oxo-3-pentynoate (*16*). Negative cooperativity was detected in the noncovalent interaction of the substrate analogue *cis,cis*-muconate with the catalytically damaged R39Q mutant of 4-OT (*2*), but not with the wild-type enzyme (*11*). Hence, anticooperative interactions have heretofore been detected in only the covalent inactivation of 4-OT, or with a mutated enzyme.

Our studies establish the substoichiometric binding of equilibrium mixtures of reactive substrates, intermediates,

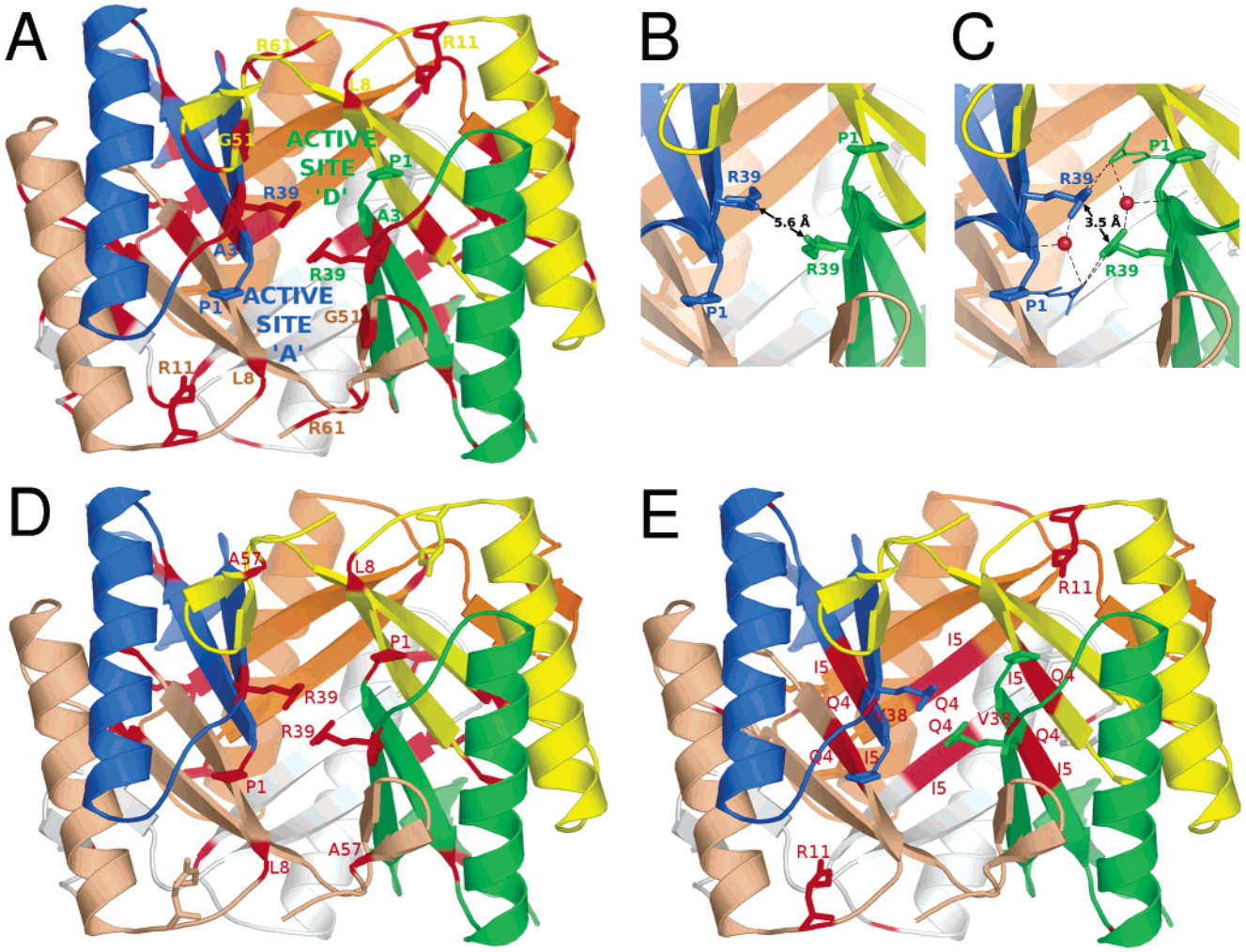

FIGURE 9: Mapping of the resonances of 4-OT, split or broadened by ligand binding, onto the X-ray structure of the affinity-labeled enzyme (PDB entry 1BJP). (A) Mapping of the split resonances at saturating concentrations of active intermediates 2-HM and 2-HPD (Table 1). While all residues with split signals are colored red, for clarity, only seven representative residues per active site are labeled. The color coding for each subunit is given in the legend of Figure 2. (B) Enlargement of the active site regions of the A and D subunits of free 4-OT (PDB entry 1OTF) showing the interaction of R39 of the D subunit [R39(D)] with R39 of the A subunit [R39(A)]. (C) X-ray structure of the same region of affinity-labeled 4-OT showing the affinity label (thin sticks) attached to the P1 residues of both subunits. Bound water molecules are represented by red balls, and hydrogen bonds are represented by dashed lines. Note the decrease in distance and change in orientation of both R39(A) and R39(D) in the affinity-labeled enzyme. (D) Mapping of resonances broadened by both active intermediates and the unreactive intermediate analogues (red residues). (E) Resonances broadened *only* by active intermediates and *not* by unreactive intermediate analogues (red residues).

and products to the wild-type enzyme, with approximately half-of-the-sites stoichiometry. Similar half-site binding stoichiometry was found with the dicarboxylate intermediate analogue and potent competitive inhibitor (2*E*)-FM. Because of the weak binding of the monocarboxylate intermediate analogues (2*E*)- and (2*Z*)-FPD under the conditions of the NMR titrations, these ligands usually did not give well-defined binding stoichiometries. Active site binding of all ligands is indicated by two observations: they all broadened the P1 N resonance, and they all downshifted the guanidinium Nϵ resonances of R11 and R39, residues which play major roles in catalysis (Figure 1) (*2*, *5*, *6*).

Independent evidence for negative cooperativity, and for the accompanying development of structural asymmetry on ligand binding (*27*), was the detection of *splitting* of resonances of 4-OT in the saturated enzyme−ligand complexes. These split resonances (Tables 1 and 3), which are mapped onto the X-ray structure of 4-OT (*4*) in Figure 9A, are assigned to contact and second-shell residues surrounding the active site, as well as to more remote residues (see below).

On the basis of the structure of 4-OT, nonclassical substrate binding might be expected. Both a nonliganded X-ray structure (PDB entry 1OTF) (*3*) and an X-ray structure in which all six active sites are covalently modified by 2-oxo-3(*E*)-pentenoate at P1 (PDB entry 1BJP) (*4*) have been determined. The two structures are very similar (Cα rmsd = 0.80 Å), and the solution secondary structure of nonliganded 4-OT is unchanged when it is complexed with the weak ligand *cis*,*cis*-muconate (*11*). Because the X-ray structure of the free enzyme does not show the three C-terminal residues (*3*), this discussion will be based primarily on the structure of the affinity-labeled enzyme (*4*).

The 4-OT homohexamer is a trimer of dimers, with each dimer consisting of two antiparallel α-helices on one side of a four-stranded mixed β-sheet (Figure 2). Each of the six active sites of this homohexamer consists of catalytic components from three subunits (*4*). The major catalytic

components of 4-OT are P1, the general base, R11′, which binds the 6-carboxylate of the substrate to anchor and orient it, and R39″, which binds the 1-carboxylate and 2-carbonyl group of the substrate (Figure 1). The catalytic components are positioned in a hydrophobic cavity with a local effective dielectric constant of 14 (*8*), partially covered by a β-hairpin, F50′ to A57′. Active site A, defined as containing P1(A) (i.e., P1 of the A subunit), receives both R11(B) and the β-hairpin [F50(B) to A57(B)] from subunit B, its dimeric partner. Active site A receives R39(D) from subunit D, the nearer subunit of the adjacent dimer (Figure 2). Indeed, the nearest active site to site A is active site D, as indicated by the distance of 13.5 Å between the nitrogens of P1(A) and P1(D). The other four active sites, B, C, E, and F, are 21.3, 25.4, 25.4, and 30.4 Å, respectively, from site A. By symmetry, analogous statements can be applied to active sites B−F (Figure 2).

The key piece of evidence indicating that active site A uses R39(D) from across the dimer−dimer interface, rather than its own R39(A), is provided by the hydrogen bonding distances from Nη and Nϵ of R39(D) to the carboxylate oxygen (2.6 Å) and carbonyl oxygen (2.9 Å), respectively, of 2-oxo-3(*E*)-pentenoate, covalently attached to P1(A) (Figure 2C) (*4*). Two-fold greater distances of 5.1 and 7.0 Å, respectively, were found from the Nη and Nϵ resonances of R39(A) to these oxygens. Nevertheless, R39(A) does interact *indirectly* with the carbonyl oxygen of 2-oxo-3(*E*)-pentenoate covalently attached to P1(A) through a water molecule which is positioned to assist in polarizing the carbonyl group (Figure 9C) (*4*).

It is noteworthy that the cationic guanidinium group of R39(D) is near that of R39(A) in the free enzyme with R39-(D) Cζ 5.0 Å from R39(A) Nη, and an average distance of 5.6 Å between the two guanidinium groups (Figure 9B) (*3*). In the affinity-labeled enzyme (*4*) in which all six sites are occupied, mimicking the enzyme fully populated with substrate, these planar guanidinium groups move closer and become stacked, with R39(D) Cζ at an aromatic stacking distance of 3.5 Å from R39(A) Nη (Figure 9C)[4] (*4*). In aqueous solution, guanidinium at a very high concentration (3 M) shows a weak tendency to stack (+1.3 kcal/mol) (*28*). On 4-OT, this reversible stacking interaction could provide a minimal pathway for the effect of substrate binding to active site A to be transmitted allosterically to the nearest active site, D.

To understand the negative cooperativity, however, requires the elucidation of not only the allosteric pathway but also the allosteric message from site A to site D, which in this case is "bind the substrate more weakly". How is this accomplished? When site A is occupied, the binding of a second substrate at site D induces the stacking of the cationic guanidinium group of R39(A) onto that of R39(D). This electrostatically unfavorable interaction would weaken substrate binding at site D. Using the local dielectric constant of 14 at the active site of 4-OT (*8*), we estimate, from the Born equation, an unfavorable free energy of +1.0 kcal/mol for decreasing the distance between the guanidinium groups of R39(A) and R39(D) from its average value of 5.6 Å in the free enzyme to a stacking distance of 3.5 Å. While the repulsion between R39(D) and R39(A) alone would thereby weaken substrate binding by 5.6-fold, two observations indicate that other effects also contribute to negative cooperativity. First, the binding of the second substrate must be weakened by at least 40-fold to explain the observed half-of-the-sites binding stoichiometry, as estimated from the titration data (Figures 6−8) which showed clear end points and no additional binding sites at ligand concentrations up to 13 mM. Second, the R39Q mutant shows anticooperative binding of the substrate analogue, *cis,cis*-muconate, with an 8.4-fold greater K_D at the second site than at the tight site (*2*). Simple additivity of this effect and the effect of the R39-(D)···R39(A) repulsion would weaken ligand binding by 47-fold, an amount sufficient to explain the half-of-the-site binding stoichiometries detected in this work.

Weaker substrate binding at the second site could result from faster substrate dissociation. Faster dissociation of the product (which resembles the substrate) would minimize product inhibition and thereby promote catalysis via a reciprocating mechanism in which substrate binding at site A would accelerate dissociation of the product from site D (*29*−*31*). Such half-site binding of substrates is not incompatible with Michaelis−Menten kinetics (*29*−*31*).

Especially important are residues which show splitting of their resonances at maximal ligand occupancy in the NMR titration experiments, indicative of induced asymmetry between subunits (Tables 1 and 3 and Figure 9A). While some of these residues cluster around and include R39, others are more remote. For example, in active site A, defined as containing P1(A), R39(D) is near L35(D) (5.9 Å), T36(D) (4.3 Å), and G53(B) (5.0 Å). However, R11(B) (13.5 Å), S12(B) (20.6 Å), and G48(B) (13 Å) are farther from R39-(D), even though R11(B) helps to anchor the bound dicarboxylate substrate at site A (Figure 1). All of these residues may participate in the allosteric interactions between the A, B, and D subunits, thereby contributing to the negative cooperativity. By symmetry, the same arguments can be made for all of the other active sites. Interestingly, no resonance splittings occur in the α-helices (Figure 9A), indicating that no structural asymmetries are induced in the helices by ligand binding, although some helical residues show small chemical shift changes (Figure 3). The α-helices are on the outside of the 4-OT molecule (Figure 2) (*4*), providing structural support by helping to hold together the paired monomers in each dimer, while the active sites are located more deeply, and receive no catalytic residues from the helices.

Recent quantum mechanical/molecular mechanical calculations of the mechanism of 4-OT (*15*) suggested that both arginines R39(D) and R39(A) are major contributors to transition state stabilization at site A. However, the contribution of R39(A) was not independently evaluated by omitting it from the computation. Moreover, the chemical mechanism by which R39(A), which participates directly in catalysis in active site D, might contribute to catalysis in site A was not discussed. As noted above, R39(A) interacts indirectly with the carbonyl oxygen of 2-oxo-3(*E*)-pentendioate covalently attached to P1(A) through a water molecule which is positioned to assist in polarizing the carbonyl group (Figure 9C). This water was computed to contribute 2.0 kcal/mol to transition state stabilization by 4-OT (*15*). In addition, our

[4] While P1 shows no change in position or orientation in the affinity-labeled enzyme (PDB entry 1BJP) (*4*), the guanidinium group of R11 shows a change in orientation (χ_4) but not in position.

previous studies of the R39Q mutant (*2*, *9*), together with the structural information discussed above, indicate that the R39(D)···R39(A) repulsion contributes significantly but not exclusively to the negative cooperativity and induced asymmetry in substrate binding by 4-OT.

Of the seven active site residues in direct contact with the bound intermediate [P1(A), I2(A), L8(B), R11(B), R61(B), S37(D), and R39(D)],[5] these NMR titrations with equilibrium mixtures of substrate, intermediate, and product showed changes in chemical shifts of three of these residues (R11 NH, R11 NϵH, R39 NH, R39 Nϵ, and S37 NH), and broadening of that of P1 N. Of the 10 second-shell residues surrounding the active site [L31(A), A33(A), V38(A), R39-(A), H6(B), I7(B), P34(B), M45(B), F50(B), and I52(B)],[5] six showed significant chemical shift changes (I5 NH, H6 NH, L8 NH, V38 NH, R39 NH, R39 Nϵ, and M45 NH) (Figures 3A,B and 4). Very similar chemical shift changes were induced by the binding of dicarboxylate and monocarboxylate analogues of the reactive intermediates.

The broadening of resonances on ligand binding suggests dynamic behavior such as chemical exchange. Indeed, preliminary comparisons of 600 and 800 MHz spectra show greater broadenings of backbone NH and Arg NϵH resonances at 800 MHz, consistent with chemical exchange.[6] Resonances broadened by *both* reactive intermediates and their unreactive analogues were those of P1 N, L8 NH, R39 NH, R39 Nϵ, and A57 NH, suggesting that these residues (mapped in Figure 9D) become mobilized and undergo chemical exchange during ligand binding and dissociation from the active sites. Resonances broadened *only* by active intermediates and *not* by unreactive analogues were the Q4 NH, I5 NH, R11 NH, R11 NϵH [with (2*E*)-HPD only], and V38 NH resonances, suggesting that these residues (mapped in Figure 9E) undergo chemical exchange *only* during catalysis. Exchange during catalysis might well be expected for R11, a catalytic residue, for V38, which is adjacent to catalytic residue R39, and for I5(B), a second-shell residue which approaches P1(A) at an N to N distance of 4.7 Å, but not for Q4(A) which is 10.1 Å from P1(A). However, the backbone NH of Q4(A) interacts via hydrogen bonding with its symmetry-related partner, Q4(B), at the center of the intersubunit, antiparallel β-sheet which, together with the paired α-helices, forms a scaffold to stabilize the A−B dimer. Since catalysis involves major contributions of catalytic residues from subunit B to subunit A of the dimer, and vice versa, motion during catalysis may thereby be transmitted through this scaffold.

ACKNOWLEDGMENT

We are grateful to Dr. Ananya Majumdar for help with the NMR instrumentation.

[5] Active site residues in contact with the bound intermediate were identified by model building based on the X-ray structure of the affinity-labeled enzyme (PDB entry 1BJP) (*4*) using PyMOL (*32*). The covalent adduct 2-oxo-3(*E*)-pentenoate was removed; protons were added, and (2*E*,4*E*)-HM was docked into the active site, avoiding overlaps. Contact residues were identified as those with atoms within 2.4 Å of the bound intermediate, and second-shell residues were defined as those with atoms between 2.5 and 4.8 Å from the bound intermediate. The process was repeated, docking (2*Z*,4*E*)-HM, which added one contact residue, R11, and all contact and second-shell residues are reported.

[6] H. F. Azurmendi and A. S. Mildvan, unpublished observations, 2004. Analyses of the relaxation rates will be the subject of a future paper.

REFERENCES

1. Whitman, C. P. (2002) The 4-oxalocrotonate tautomerase family of enzymes: How nature makes new enzymes using a $\beta-\alpha-\beta$ structural motif, *Arch. Biochem. Biophys. 402*, 1−13.
2. Harris, T. K., Czerwinski, R. M., Johnson, W. H., Jr., Legler, P. M., Abeygunawardana, C., Massiah, M. A., Stivers, J. T., Whitman, C. P., and Mildvan, A. S. (1999) Kinetic, stereochemical, and structural effects of mutations of the active site arginine residues in 4-oxalocrotonate tautomerase, *Biochemistry 38*, 12343−12357.
3. Subramanya, H. S., Roper, D. I., Dauter, Z., Dodson, E. J., Davies, G. J., Wilson, K. S., and Wigley, D. B. (1996) Enzymatic ketonization of 2-hydroxymuconate: Specificity and mechanism investigated by the crystal structures of two isomerases, *Biochemistry 35*, 792−802.
4. Taylor, A. B., Czerwinski, R. M., Johnson, W. H., Jr., Whitman, C. P., and Hackert, M. L. (1998) Crystal structure of 4-oxalocrotonate tautomerase inactivated by 2-oxo-3-pentynoate at 2.4 Å resolution: Analysis and implications for the mechanism of inactivation and catalysis, *Biochemistry 37*, 14692−14700.
5. Stivers, J. T., Abeygunawardana, C., Mildvan, A. S., Hajipour, G., Whitman, C. P., and Chen, L. H. (1996) Catalytic role of the amino-terminal proline in 4-oxalocrotonate tautomerase: Affinity labeling and heteronuclear NMR studies, *Biochemistry 35*, 803−813.
6. Stivers, J. T., Abeygunawardana, C., Mildvan, A. S., Hajipour, G., and Whitman, C. P. (1996) 4-Oxalocrotonate tautomerase: pH dependence of catalysis and pK_a values of active site residues, *Biochemistry 35*, 814−823.
7. Czerwinski, R. M., Johnson, W. H., Jr., Whitman, C. P., Harris, T. K., Abeygunawardana, C., and Mildvan, A. S. (1997) Kinetic and structural effects of mutations of the catalytic amino-terminal proline in 4-oxalocrotonate tautomerase, *Biochemistry 36*, 14551−14560.
8. Czerwinski, R. M., Harris, T. K., Massiah, M. A., Mildvan, A. S., and Whitman, C. P. (2001) The structural basis for the perturbed pK_a of the catalytic base in 4-oxalocrotonate tautomerase: Kinetic and structural effects of mutations of Phe-50, *Biochemistry 40*, 1984−1995.
9. Czerwinski, R. M., Harris, T. K., Johnson, W. H., Jr., Legler, P. M., Stivers, J. T., Mildvan, A. S., and Whitman, C. P. (1999) Effects of mutations of active site arginine residues in 4-oxalocrotonate tautomerase on the pK_a values of active site residues and on the pH dependence of catalysis, *Biochemistry 38*, 12358−12366.
10. Stivers, J. T., Abeygunawardana, C., Whitman, C. P., and Mildvan, A. S. (1996) 4-Oxalocrotonate tautomerase, a 41-kDa homohexamer: Backbone and side-chain resonance assignments, solution secondary structure, and location of active site residues by heteronuclear NMR spectroscopy, *Protein Sci. 5*, 729−741.
11. Stivers, J. T., Abeygunawardana, C., Mildvan, A. S., and Whitman, C. P. (1996) ^{15}N NMR relaxation studies of free and inhibitor-bound 4-oxalocrotonate tautomerase: Backbone dynamics and entropy changes of an enzyme upon inhibitor binding, *Biochemistry 35*, 16036−16047.
12. Fitzgerald, M. C., Chernushevich, I., Standing, K. G., Kent, S. B. H., and Whitman, C. P. (1995) Total chemical synthesis and catalytic properties of the enzyme enantiomers L- and D-4-oxalocrotonate tautomerase, *J. Am. Chem. Soc. 117*, 11075−11080.
13. Cisneros, G. A., Wang, M., Silinski, P., Fitzgerald, M. C., and Yang, W. (2004) The protein backbone makes important contributions to 4-oxalocrotonate tautomerase enzyme catalysis: Understanding theory from experiment, *Biochemistry 43*, 6885−6892.
14. Metanis, N., Brik, A., Dawson, P. E., and Keinan E. (2004) Electrostatic interactions dominate the catalytic contribution of Arg39 in 4-oxalocrotonate tautomerase, *J. Am. Chem. Soc. 126*, 12726−12727.
15. Cisneros, G. A., Liu, H., Zhang, Y., and Yang, W. (2003) Ab initio QM/MM study shows there is no general acid in the reaction catalyzed by 4-oxalocrotonate tautomerase, *J. Am. Chem. Soc. 125*, 10384−10393.
16. Johnson, W. H., Jr., Czerwinski, R. M., Fitzgerald, M. C., and Whitman, C. P. (1997) Inactivation of 4-oxalocrotonate tautomerase by 2-oxo-3-pentynoate, *Biochemistry 36*, 15724−15732.
17. Eisenmesser, E. Z., Bosco, D. A., Akke, M., and Kern, D. (2002) Enzyme dynamics during catalysis, *Science 295*, 1520−1523.

18. Wolf-Watz, M., Thai, V., Henzler-Wildman, K., Hadjipavlou, G., Eisenmesser, E. Z., and Kern, D. (2004) Linkage between dynamics and catalysis in a thermophilic-mesophilic enzyme pair, *Nat. Struct. Mol. Biol. 11*, 945−949.
19. Azurmendi, H. F., Whitman, C. P., Miller, S. G., and Mildvan, A. S. (2004) Half site binding of substrates and inhibitors to 4-oxalocrotonate tautomerase, 228th American Chemical Society National Meeting, Philadelphia, PA, August 22−26, 2004, Abstract BIOL 99.
20. Whitman, C. P., Aird, B. A., Gillespie, W. R., and Stolowich, N. J. (1991) Chemical and enzymatic ketonization of 2-hydroxymuconate, a conjugated enol, *J. Am. Chem. Soc. 113*, 3154−3162.
21. Lian, H., and Whitman, C. P. (1993) Ketonization of 2-hydroxy-2,4-pentadienoate by 4-oxalocrotonate tautomerase: Implications for the stereochemical course and the mechanism, *J. Am. Chem. Soc. 115*, 7978−7984.
22. Johnson, W. H., Jr., Wang, S. C., Stanley, T. M., Czerwinski, R. M., Almrud, J. J., Poelerands, G. J., Murzin, A. G., and Whitman, C. P. (2004) 4-Oxalocrotonate tautomerase, its homologue, YwhB, and active vinylpyruvate hydratase: Synthesis and evaluation of 2-fluoro substrate analogues, *Biochemistry 43*, 10490−10501.
23. Waddell, W. J. (1956) A simple ultraviolet spectrophotometric method for the determination of protein, *J. Lab. Clin. Med. 48*, 311−314.
24. Delaglio, F., Grzesiek, S., Vuister, G. W., Zhu, G., Pfeifer, J., and Bax, A. (1995) NMRPipe: A multidimensional spectral processing system based on UNIX pipes, *J. Biomol. NMR 6*, 277−293.
25. Goddard, T. D., and Kneller, D. G. (2004) *Sparky 3*, University of California, San Francisco.
26. Saraswat, V., Massiah, M. A., Lopez, G., Amzel, L. M., and Mildvan, A. S. (2002) Interactions of the products 8-oxo-dGMP, dGMP, and pyrophosphate with the MutT nucleoside triphosphate pyrophosphohydrolase, *Biochemistry 41*, 15566−15577.
27. Koshland, D. E., Jr. (1970) The molecular basis for enzyme regulation. *The Enzymes*, 3rd ed. (Boyer, P. D., Ed.) Academic Press, pp 341−396, New York.
28. Mason, P. E., Neilson, G. W., Enderby, J. E., Saboungi, M.-L., Dempsey, C. E., Mackerrell, A. D., Jr., and Brady, J. W. (2004) The structure of aqueous guanidinium solutions, *J. Am. Chem. Soc. 126*, 11462−11470.
29. Mueggler, P. A., and Wolfe, R. G. (1978) Malate dehydrogenase. Kinetic studies of substrate activation of the supernatant enzyme by L-malate, *Biochemistry 17*, 4615−4620.
30. Mueggler, P. A., Dahlquist, F. W., and Wolfe, R. G. (1975) Malate dehydrogenase, anticooperative NADH, and L-malate binding in ternary complexes with supernatant pig heart enzyme, *Biochemistry 14*, 3490−3497.
31. Segel, I. H. (1975) *Enzyme kinetics*, pp 377−387, John Wiley and Sons, New York.
32. DeLano, W. L. (2004) *PyMOL*, DeLano Scientific, San Carlos, CA.

BI0502590